EARTHQUAKE ENGINEERING AND STRUCTURAL DYNAMICS, VOL. 25, 1391–1404 (1996)

SCATTERING OF SH WAVES IN MULTILAYERED MEDIA WITH IRREGULAR INTERFACES

GANG DING* AND MARIJAN DRAVINSKI†
University of Southern California, Los Angeles, California 90089-1453, U.S.A.

SUMMARY

An indirect boundary integral equation method is used to investigate the scattering of elastic SH waves in a multilayered media with irregular interfaces. An extensive parametric error analysis is performed in order to assess the convergence of the proposed method. Subsequently, the numerical results for both steady-state and transient surface response are given for one- and two-layer models.

KEY WORDS: scattering; SH-waves; irregular layers

INTRODUCTION

Scattering in multilayered media with irregular interfaces has many practical applications in geophysics and non-destructive testing. While wave propagation in media with flat interfaces have been studied by many investigators in the past (e.g. References 1–7), there have been few studies dealing with irregular layers (e.g. References 8–11). Aki and Larner[8] studied the steady-state surface response of a one-layer lateral varying structure with moderately shallow slopes subjected to an incident harmonic SH wave. They used a technique based on the Rayleigh hypothesis. Koketsu *et al.*[12] extended the Aki–Larner technique to a multilayered case. Kennett[13,14] introduced the concept of reflection and transmission operators in the context of interface problems. This work was later generalized by Chen[11] to synthesize the seismograms of the multilayered media by incorporating the T-matrix method.[15]

Using the boundary integral equation approach, Dravinski,[16] and Eshraghi and Dravinski,[17,18] investigated wave motion in finite dipping layers for two- and three-dimensional models.

This work is an extension of the investigation done by Dravinski,[16] who considered scattering of SH waves by multiple finite dipping layers of arbitrary shape. Here the problem is extended to multiple infinitely long layers of irregular shape.

STATEMENT OF THE PROBLEM

The geometry of the problem is depicted in Figure 1. The model consists of a set of elastic layers overlaying a half-space. The interfaces between the layers are assumed to be irregular but sufficiently smooth without sharp corners. The free surface is flat. The spatial domains are denoted by $D_j, j = 1, \ldots, N$ while the irregular interfaces are designated by C_i, $i = 1, 2, \ldots, N-1$. The top free surface is denoted by S_F. Each irregular interface is assumed to vary around the corresponding flat reference surface with depth z_i, $i = 1, 2, \ldots, N-1$. The flat reference surfaces are denoted by S_i, $i = 1, 2, \ldots, N-1$. If the ith irregular interface is flat, then C_i will coincide with the reference surface S_i.

*Graduate Student
†Professor

CCC 0098–8847/96/121391–14

Received 27 July 1995
Revised 11 June 1996

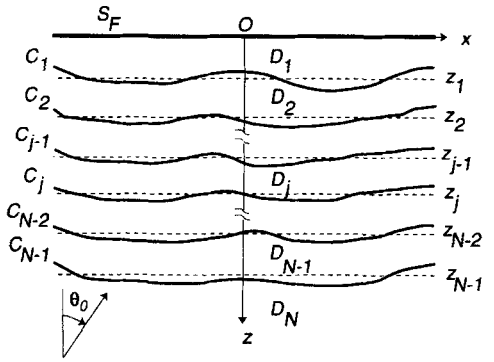

Figure 1. Model geometry

Material of the media is assumed to be elastic, homogeneous and isotropic. The Cartesian co-ordinates with origin at O are denoted by x, y and z. The system is subjected to a plane harmonic SH incident wave with an off-vertical angle of incidence θ_0. For the antiplane strain problem, the motion of the media takes place along the y-axis only, i.e. $\mathbf{u} = (0, v, 0)$. Therefore, in the absence of body forces, the equation of motion is given by

$$(\nabla^2 + k_j^2)\, v_j(x, z, \omega) = 0; \quad j = 1, \ldots, N, \quad \nabla^2 = \frac{\partial^2}{\partial x^2} + \frac{\partial^2}{\partial z^2} \tag{1}$$

where

$$k_j = \frac{\omega}{\beta_j}; \quad \beta_j^2 = \frac{\mu_j}{\rho_j}; \quad \lambda_j = \frac{2\pi\beta_j}{\omega} \tag{2}$$

Here v is the only non-zero component of the displacement field acting along the y-axis, k_j, β_j and λ_j represent wave number, shear wave velocity and wavelength in the jth layer, respectively, ω is the circular frequency, μ is the shear modulus, and ρ is the density.

The perfect bonding conditions along the interfaces C_j can be written as

$$v_j = v_{j-1}; \quad \mathbf{r} \in C_j; \quad j = 1, 2, \ldots, N-1 \tag{3}$$

$$\mu_j \frac{\partial v_j}{\partial n} = \mu_{j-1} \frac{\partial v_{j-1}}{\partial n}; \quad \mathbf{r} \in C_j; \quad j = 1, 2, \ldots, N-1 \tag{4}$$

where $\mathbf{n}$ denotes the unit normal to C_j, respectively. The traction-free boundary condition on the top surface S_F reduces to

$$\frac{\partial v_1}{\partial z} = 0, \quad \mathbf{r} \in S_F \tag{5}$$

The incident wave is assumed of the form

$$v^{\text{inc}} = e^{-ik_0(x \sin\theta_0 - z\cos\theta_0) + i\omega t}; \quad i = \sqrt{-1} \tag{6}$$

The factor $e^{i\omega t}$ will be omitted in the following.

SOLUTION OF THE PROBLEM

Steady-state problem

The total wave field in the multi-layer media can be expressed as a superposition of the free-field and scattered wave field according to

$$v_j = v_j^{\mathrm{ff}} + v_j^{\mathrm{s}}; \quad j = 1, \ldots, N \tag{7}$$

in which the superscript ff denotes the free-field of the flat-layer system, and s denotes the scattered wave field caused by the irregular interfaces.

The free-field in each layer is given by

$$v_j^{\mathrm{ff}} = A_j \mathrm{e}^{-\mathrm{i}k_j(x\sin\theta_j - z\cos\theta_j)} + B_j \mathrm{e}^{-\mathrm{i}k_j(x\sin\theta_j + z\cos\theta_j)}; \quad (x, z) \in D_j, j = 1, \ldots, N \tag{8}$$

where A_j and B_j are the amplitudes of up and down propagating SH waves in the domain D_j. The parameters A_j, B_j and θ_j are known (e.g. Reference 19).

The unknown scattered wave field can be expressed in terms of single-layer potentials (e.g. References 20 and 21):

$$v_1^{\mathrm{s}} = \int_{C_1^+} p_1(\mathbf{r}_0)\, G_1(\mathbf{r}, \mathbf{r}_0)\, \mathrm{d}\mathbf{r}_0; \quad \mathbf{r} \in D_1 \tag{9}$$

$$v_j^{\mathrm{s}} = \int_{C_{j-1}^-} q_j(\mathbf{r}_0)\, G_j(\mathbf{r}, \mathbf{r}_0)\, \mathrm{d}\mathbf{r}_0 + \int_{C_j^+} p_j(\mathbf{r}_0)\, G_j(\mathbf{r}, \mathbf{r}_0)\, \mathrm{d}\mathbf{r}_0; \quad \mathbf{r} \in D_j, j = 2, \ldots, N-1 \tag{10}$$

$$v_N^{\mathrm{s}} = \int_{C_{N-1}^-} q_{N-1}(\mathbf{r}_0)\, G_{N-1}(\mathbf{r}, \mathbf{r}_0)\, \mathrm{d}\mathbf{r}_0; \quad \mathbf{r} \in D_N \tag{11}$$

where q_j and p_j are the unknown density functions. The functions G_j are Green's functions for the line load in the half-space, and they satisfy the following equations:[16]

$$(\nabla^2 + k_j^2)\, G_j(\mathbf{r}, \mathbf{r}_0) = \delta(|\mathbf{r} - \mathbf{r}_0|); \quad j = 1, 2, \ldots, N \tag{12}$$

$$\frac{\partial G_j}{\partial z} = 0 \quad \text{at } z = 0 \tag{13}$$

with $\delta(.)$ being the Dirac delta function. The Green functions are given by[22]

$$G_j(\mathbf{r}, \mathbf{r}_0) = \frac{\mathrm{i}}{4}[H_0^2(k_j\sigma_1) + H_0^2(k_j\sigma_2)]; \quad j = 1, 2, \ldots, N \tag{14}$$

$$\sigma_1 = \sqrt{(x - x_0)^2 + (z - z_0)^2}; \quad \sigma_2 = \sqrt{(x - x_0)^2 + (z + z_0)^2} \tag{15}$$

in which $H_0^2(\cdot)$ denotes the Hankel function of the second kind and order zero. The auxiliary surfaces C_j^+ and C_j^- are defined below and above the corresponding interface C_j[16]. It should be noted that the unknown scattered wave field representation (Equations. (9)–(11)) involves improper integrals since the interfaces $C_j^{\pm}$ extend to infinity.

If the scattered wave field is assumed in terms of discrete line sources, then for the jth layer

$$q_j(\mathbf{r}) = a_{m_{j-1}}^j\, \delta(|\mathbf{r} - \mathbf{r}_{m_{j-1}}|); \quad \mathbf{r} \in D_j; \ \mathbf{r}_{m_{j-1}} \in C_{j-1}^-$$
$$j = 2, \ldots, N-1; \quad m_{j-1} = 1, 2, \ldots, M_{j-1} \tag{16}$$

$$p_j(\mathbf{r}) = b_{l_j}^j\, \delta(|\mathbf{r} - \mathbf{r}_{l_j}|); \quad \mathbf{r} \in D_j; \ \mathbf{r}_{l_j} \in C_j^+$$
$$j = 2, \ldots, N-1; \quad l_j = 1, 2, \ldots, L_j \tag{17}$$

where $a_{m_j}^j$ and $b_{l_j}^j$ denote the unknown source intensities, and M_j and L_j represent the order of approximation, that is the number of discretized sources, along the auxiliary surfaces C_j^+ and C_j^-, respectively. In doing so the infinite integrals in Equations (9)–(11) are replaced by the finite integrals and, consequently, the number of sources which represent the scattered waves becomes finite as well. The orders of approximations M_j and L_j are still to be determined.

Substitution of equations (16) and (17) into (9)–(11) yields the scattered wave field in the following form:

$$v_1^s = \sum_{l_1=1}^{L_1} b_{l_1}^1 G_1(\mathbf{r}, \mathbf{r}_{l_1}); \quad \mathbf{r} \in D_1; \quad \mathbf{r}_{l_1} \in C_1^+ \tag{18}$$

$$v_j^s = \sum_{m_{j-1}=1}^{M_{j-1}} a_{m_{j-1}}^j G_j(\mathbf{r}, \mathbf{r}_{m_{j-1}}) + \sum_{l_j=1}^{L_j} b_{l_j}^j G_j(\mathbf{r}, \mathbf{r}_{l_j})$$

$$\mathbf{r} \in D_j; \quad j = 2, \ldots, N-1; \quad \mathbf{r}_{m_{j-1}} \in C_{j-1}^-; \quad \mathbf{r}_{l_j} \in C_j^+ \tag{19}$$

$$v_N^s = \sum_{m_1=1}^{M_{N-1}} a_{m_{N-1}}^N G_N(\mathbf{r}, \mathbf{r}_{m_{N-1}}); \quad \mathbf{r} \in D_N; \quad \mathbf{r}_{m_{N-1}} \in C_{N-1}^- \tag{20}$$

It should be pointed out that instead of discrete sources the scattered waves can be expressed in terms of continuously distributed sources along the boundaries (e.g. Reference 23). The approach used in this work avoids the problems associated with singularities of Green's functions at the cost of introducing the so-called auxiliary interfaces $C^{+/-}$. Use of continuously distributed sources, on the other hand, requires special care in handling these singularities.

Source intensities for scattered wave field

The scattered wave field (18)–(20) satisfies the equation of motion (1) and the stress free boundary condition (5). The unknown source intensities of the scattered wave field are determined by imposing the displacement and tractions continuity conditions (3), (4). This implies that

$$v_j^s - v_{j+1}^s = v_{j+1}^{ff} - v_j^{ff} \tag{21}$$

$$\mu_j \frac{\partial v_j^s}{\partial n} - \mu_{j+1} \frac{\partial v_{j+1}^s}{\partial n} = \mu_{j+1} \frac{\partial v_{j+1}^{ff}}{\partial n} - \mu_j \frac{\partial v_j^{ff}}{\partial n}$$

$$\mathbf{r} \in C_j, \quad j = 1, 2, \ldots, N-1 \tag{22}$$

Choosing N_j collocation points along interfaces C_j, the continuity conditions (21), (22) can be written in the following form:

$$\mathbf{Aa} = \mathbf{f} \tag{23}$$

In equation (23), the matrix $\mathbf{A}$ of size $2N \times (M + L)$ and the forcing vector $\mathbf{f}(2N \times 1)$ are known, while the unknown source intensities of the discrete sources are incorporated in the vector $\mathbf{a}$. Equation (23) is solved for the unknown coefficient vector $\mathbf{a}$ in the least-squares sense using the QR decomposition, e.g. Reference 24.

Therefore, the boundary conditions (5) on the surface of the half-space S_F are satisfied exactly, while the continuity conditions (3), (4) are satisfied in the least-squares sense (23) . Numerical testing shows (see the transparency test) that the best accuracy is obtained when the ratio of the number of collocation points and the number of sources $2N/(M + L) = 2{\cdot}5$. This ratio has been adopted throughout the paper. Since the number of collocation points N changes with frequency (at least ten collocation points per wavelength of the incident wave) so does the number of sources $M + L$. Consequently, the continuity conditions (23) are frequency dependent as well.

NUMERICAL RESULTS

The numerical results are presented for one- and two-layer antiplane strain models. These models incorporate most of the physical characteristics of the problem with the minimum of computational effort. For each

model, the numerical results consist of parametric error analysis, the steady-state response, and the transient response.

Parametric error analysis deals with the role of different parameters upon the surface response. The following parameters are investigated: the auxiliary surfaces $C_j^{\pm}$, the number of sources M_j and L_j, and the number of collocation points N_j along each interface C_j. These parameters are determined by minimizing an error based on the surface response iterations. The steady-state surface response is then determined by using the optimum values of the required parameters obtained in the error analysis. The transient response is obtained through the Fourier transform using the FFT technique.

Error criteria

For the error analysis all spatial variables are normalized with respect to the average depth of the lowest interface which is assumed to be unity. For the steady-state problem, the surface displacement field is normalized with respect to the corresponding free-field solution.

Since there are no exact solutions available, the surface response error is defined according to

$$E_r = \frac{\sum_{i=1}^{N_s} (|v_1^n(\mathbf{r}_i) - v_1^{n-1}(\mathbf{r}_i)|)^2}{\sum_{i=1}^{N_s} |v_1^n(\mathbf{r}_i)|^2}; \quad \mathbf{r}_i \in S_F \tag{24}$$

where N_s is the number of observation points on the surface S_F, and the superscripts n and $n-1$ represent two consecutive iterations of the surface response. When the numerical calculations converge, the error E_r should approach zero. In practice, the minimum of the error E_r is being sought. Therefore, the choice of auxiliary surfaces $C_j^{\pm}$, and the number of sources and collocation points M_j, L_j and N_j will be determined by minimizing the error E_r.

Throughout the tests, the number of observation points used to compute the error E_r is chosen to be $N_s = 40$. The observation points are equally spaced over the range of $x \in (-2, 2)$. Dimensionless frequency Ω is defined by

$$\Omega = \frac{2z_1\omega}{\pi\beta_1} \tag{25}$$

where z_1 and β_1 are the average depth and shear wave velocity of the top layer, and ω denotes the circular frequency of the incident wave.

One-layer model

The geometry of this model is depicted in Figure 2. The interface between the layer and the half-space is cosine-shaped and defined by

$$z = \begin{cases} 1 & \text{for } |x| > 0{\cdot}5 \\ 1 + 0{\cdot}05(1 + \cos 2\pi x) & \text{for } |x| \leqslant 0{\cdot}5 \end{cases} \tag{26}$$

The number of sources along the auxiliary surfaces $C^{\pm}$ are denoted by M and L, respectively. The number of collocation points along the interface is taken to be N, while the length of the interface on which the collocation points are distributed is specified by X_n. The lengths of auxiliary surfaces C^- and C^+ over which the corresponding sources are distributed are denoted by X_m and X_l, respectively, and X_I is the length of the irregular part of the interface. The maximum deviation of the irregular interface from a flat layer model is denoted by d, and z_1 is the depth of the flat-layer. The spacing between two adjacent collocation points is marked by ds and that between the auxiliary surfaces $C^{\pm}$ and the interface C by dr. Unless stated differently, the material properties are those defined in Figure 2. Since there is only one interface between the layer and half-space, the index j associated with multiple interfaces is omitted.

Parametric error analysis. First, the transparency test for a zero-scattering condition is performed. In this test, the material properties of the layer are assumed to be the same as those of the half-space. For an initial choice of the parameters ($\theta_0 = 0°$; $N = 60$, $M = L = 24$; $X_n = 2$, $X_m = X_l = 2{\cdot}1$, ds = 0·0339, dr = 0·1017,

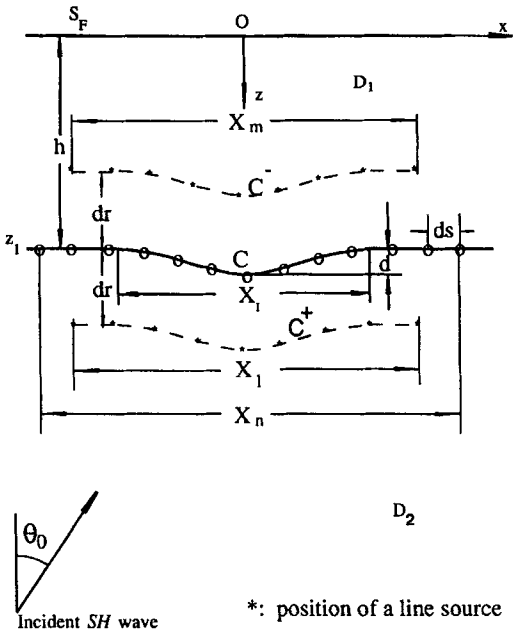

Figure 2. Geometry of the one-layer model with a cosine-shaped interface. Here, $z_1 = 1$, $X_I = 1$, $d = 0{\cdot}1$ and the material properties are $\beta_2 = \rho_2 = 1$; $\beta_1 = \rho_1 = 0{\cdot}5$

$\Omega = 2$ and $\Omega = 4$) the contribution of the scattered field is found to be negligible, and the normalized surface displacement amplitude is calculated to be equal to one. The transparency test also provides the ratio of number of rows versus number of columns in matrix **A** (equation (23)). The best accuracy is achieved for $2N/(M + L) = 2{\cdot}5$ which relates the number of collocation points (N) and the number of sources ($M + L$). Since the former is a function of the frequency (at least ten collocation points per wavelength of the incident wave) the ratio correlates the number of collocation points and the number of sources with frequency.

The second test investigates the location of the auxiliary surfaces $C^{\pm}$ relative to the interface C. J. E. Luco (private communication) proposed the following relationship between the sources and collocation points:

$$dr \doteq 3ds \tag{27}$$

where dr is the distance between the interface C and the auxiliary surface C^+ or C^-, and ds represents the spacing between two adjacent collocation points (see Figure 2).

In order to test the relationship (27), the distance ds between two adjacent collocation points is assumed to be fixed while the location of auxiliary surfaces $C^{+/-}$, specified by the parameter dr, is varied. All other parameters, such as the number of sources M and L, the number of collocation points N, the length of auxiliary surfaces X_m and X_l, and the length of interface X_n, remain the same. Therefore, from surface displacement results, the corresponding error E_r has been calculated for a range of auxiliary surfaces ($0{\cdot}05 \leqslant dr \leqslant 0{\cdot}5$). Figure 3 illustrates the results of this test for one frequency. The minimum error has been obtained for $dr = 0{\cdot}1$ which agrees very well with the optimum distance $dr = 0{\cdot}102$ predicted by equation (27). For different frequencies the results of the same test are summarized in Table I.

Apparently, for a wide range of frequencies the optimum value for dr agrees well with that obtained by equation (27). Consequently, this relationship has been accepted throughout further study of the problem.

The third test deals with the estimate of the minimum number of collocation points N. For that purpose, the error E_r is calculated for different number of collocation points N with the other parameters being fixed. The results of these calculations are depicted in Figure 4. It is interesting to note that the error E_r maintains minimum values for a wide range of N. Similar tests are done for various incident angles and frequencies. For

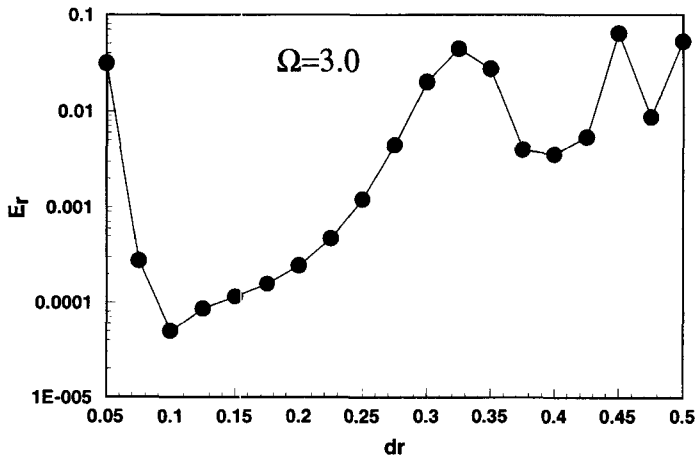

Figure 3. Error E_r as a function of the distance dr between the interface C and the auxiliary surfaces C^+ and C^- for the one-layer model subjected to a vertically incident plane harmonic wave. $N = 60$, $M = L = 24$; $X_n = 2$, $X_m = X_l = 2{\cdot}1$; $\Omega = 3$; $dr = 0{\cdot}102$ is the optimum dr proposed by the relationship ($dr \doteq 3ds$)

Table I. The optimum distance (dr) between the auxiliary surface and the interface based on minimization of the error (24). Parameters: $N = 60$, $M = L = 24$; $X_n = 2$; $X_l = 2{\cdot}1$; vertical incidence

Ω	dr
0·5	0·075
1·0	0·075
2·5	0·100
3·0	0·100
4·0	0·150
12·5	0·100
20·0	0·125

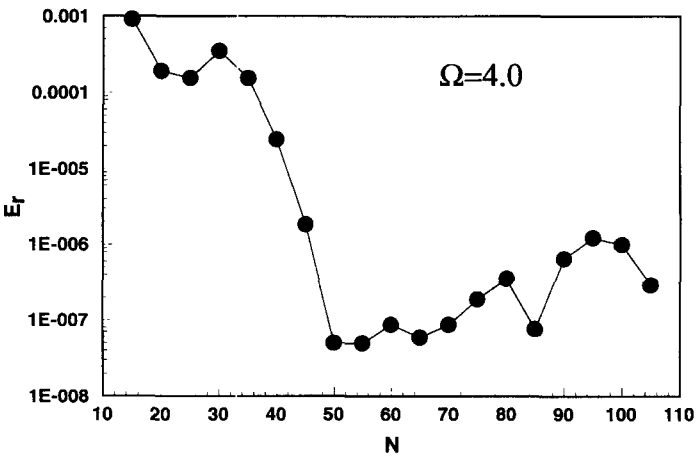

Figure 4. Error E_r as a function of the number of co location points N for the one-layer model and a vertically incident SH wave. $X_n = 2$, $X_m = X_l = 2{\cdot}1$; $dr = 3ds$; $\theta_0 = 0^\circ$; $\Omega = 4$; $M = L$, $2N/(M + L) = 2{\cdot}5$

the error $E_r \leqslant 0{\cdot}001$, these results are summarized in Table II. As expected, the number of collocation points N_{min} increases with the increase in frequency Ω. Namely, with increase in frequency, the wavelength of the incident and scattered waves becomes smaller. Therefore, the distance between two adjacent collocation points ds has to be sufficiently small to account for the shorter wavelengths in the problem. It is found in this study that there should be at least ten collocation points per wavelength of the incident wave.

The fourth test deals with the length of the interface X_n on which the collocation points are distributed (Figure 2). For this test, the maximum distance between the adjacent collocation points ds is assumed to be

$$ds_{max} = 2/N_{min} \tag{28}$$

where N_{min} is the number of collocation points given in Table II. One should recall that 2 represents the value of the interface length X_n used in the third test. Thus, the separation of the collocation points is fixed, $ds = ds_{max}$, while the parameters X_n, N, M and L are varied. For vertical incidence, the results are shown in Figure 5. It can be seen that $X_n = 2$, which is twice the length of the irregular part of the interface, is sufficient for convergence of the results. Similar results are obtained for other cases of Table II.

Therefore, the convergence tests can be summarized as follows:

(a) The transparency tests provide the initial values of the parameters in the model.
(b) Luco's relationship (27) yields the acceptable error in the scattered wave field.
(c) initially, there should be at least ten collocation points per wavelength of the incident wave along the interface, and the number of collocation points N should be increased with increase of frequency.
(d) the length of interface X_n needed for convergence of the results is about twice the length of the irregular part of the interface.

Table II. Minimum number of collocation points N for a one-layer model which results in the relative error E_r less than 0·001

N_{min}	$\Omega = 0{\cdot}5$	$\Omega = 1$	$\Omega = 2$	$\Omega = 3$	$\Omega = 4$	$\Omega = 12{\cdot}5$	$\Omega = 20$
$\theta_0 = 0°$	15	25	35	35	20	45	55
$\theta_0 = 30°$	15	20	20	30	30	50	70
$\theta_0 = 60°$	20	20	25	30	35	55	70
$\theta_0 = 85°$	20	25	30	35	35	55	85

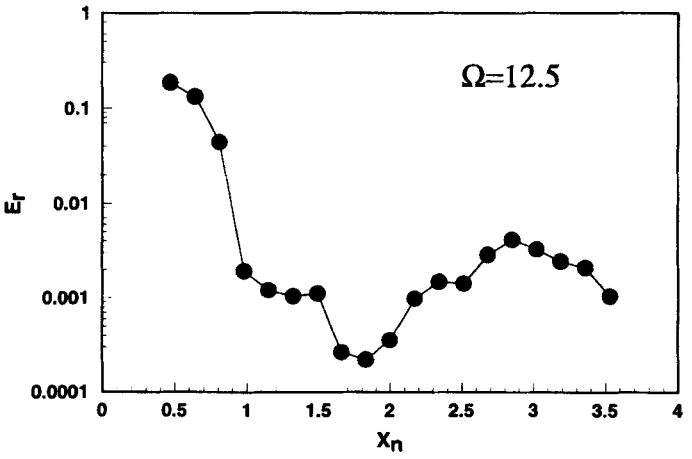

Figure 5. Error E_r as a function of length X_n over which the collocation points are applied for the one-layer model and a vertically incident SH wave. $\theta_0 = 0°$; $ds = 0{\cdot}0339$; $dr = 3ds$; $\Omega = 12{\cdot}5$; $M = L$, $2N/(M + L) = 2{\cdot}5$. $X_n = (N - 1)\,ds$

As the final test, the response of a model considered by Aki and Larner[8] is reconsidered next. Aki and Larner devised a technique to calculate elastic wave field in a half-space overlaid by a single layer with an irregular interface. Plane SH incident wave propagating from below was assumed.

The geometry of the problem studied by Aki and Larner[8] consists of a single layer where the interface between the layer and the half-space is defined (in km) by

$$z = \begin{cases} 25 & \text{for } |x| > 25 \\ 25 + 2{\cdot}5\left(1 + \cos\dfrac{\pi x}{25}\right) & \text{for } |x| \leqslant 25 \end{cases} \tag{29}$$

The velocities and densities of the layer and half-space roughly correspond to those of the crust and upper mantle, respectively. The plane SH wave with wavelength 10km in the half-space is incident from below at various incident angles.

The comparison of the numerical results obtained by the method proposed in this work with those of Aki and Larner[8] is shown in Figure 6. Relatively good agreement for the surface displacement between the two approaches is achieved. The phase delay of the surface displacement field is in excellent agreement for the two results. Therefore, the results of Figure 6 confirm the accuracy of the present method.

This completes the parametric error analysis for the one-layer model. Steady-state results for different frequencies and angles of incidence are presented next.

Steady-state response. Based on the convergence criteria developed above, the steady-state surface response for the one-layer model and a vertical incidence is shown in Figure 7. The following can be observed from the steady-state results.

1. A small deviation along the flat-layer interface may cause large surface motion amplification (up to several times of the corresponding free-field motion).

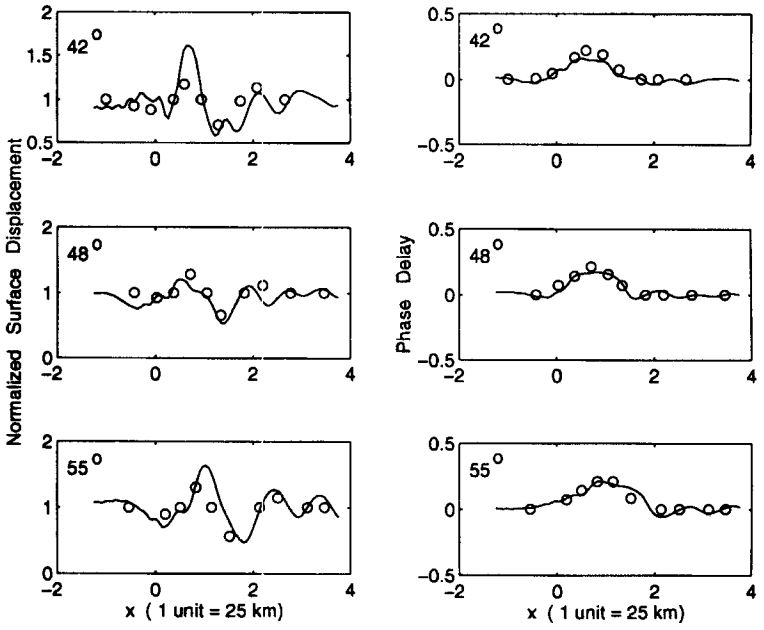

Figure 6. Comparison of normalized surface displacement and phase delay between the present approach (solid) and the Aki–Larner technique (○) for various angles of incidence. The parameters are defined as $\beta_2 = 4{\cdot}0$ km/sec, $\rho_2 = 3{\cdot}3$ g/cm^3, $\beta_1 = 3{\cdot}0$ km/sec, $\rho_1 = 2{\cdot}8$ g/cm^3, and the depth of layer $z_1 = 25$ km. The wavelength of incident wave in the half-space is 10 km which corresponds to circular frequency $\omega = 2{\cdot}5133$ sec^{-1}

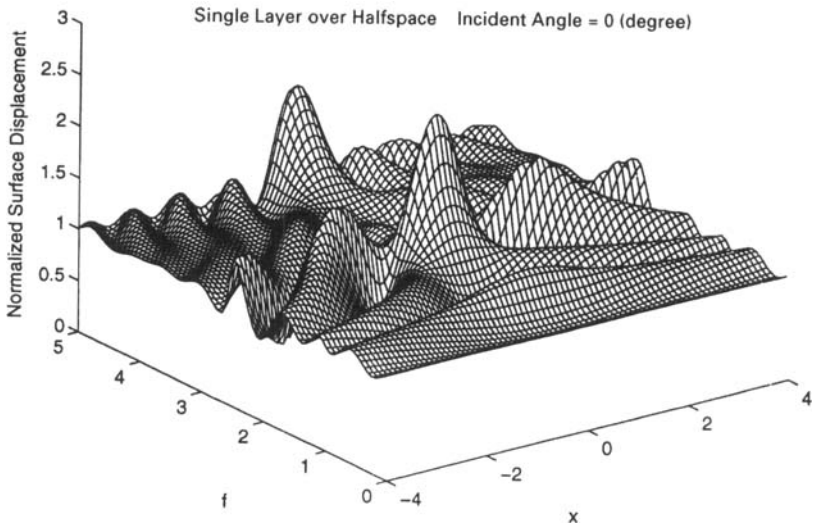

Figure 7. Normalized surface response for the one-layer model and vertically incident waves as a function of dimensionless frequency $f(=\Omega)$ and spatial variable x. $\theta_0 = 0°$; $X_n = 2$, $X_m = X_l = 2{\cdot}1$; dr = 3ds, $N = 40$ and $M = L = 16$

2. The surface displacement strongly depends upon the incident wave and the position of the site.
3. For larger values of $|x|$, the surface displacement approaches unity which corresponds to the flat-layer response. This is expected since, away from the irregularity, the scattered wave field should decrease in amplitude and the total wave field approaches the values of the free field.
4. For observation sites directly above the irregular interface, the surface response exhibits resonant features.[25] The resonant frequencies are closely related to the ones for a flat-layer model. For a vertical incidence, the first five frequencies at the site (0, 0) are found to be $\Omega_i = 1{\cdot}00$, $2{\cdot}50$, $4{\cdot}75$, $6{\cdot}50$ and $8{\cdot}50$. For the corresponding flat-layer model the resonant frequencies are $\Omega_i = 1$, 3, 5, 7 and 9. The difference between the two is attributed to the presence of the irregularity.
5. The surface motion is found to be symmetric for a vertically incident wave, thus lending further support for the validity of the calculated results.

This concludes the steady-state analysis for a one-layer model. The transient results are considered next.

Transient response. The transient response for the one-layer model (Figure 2) is obtained from the steady-state response through Fourier synthesis. Here, the response is studied for an incident SH Ricker wavelet[26] defined by

$$f(t) = (\sqrt{\pi}/2)(\tau - 0{\cdot}5)e^{-\tau}; \quad \tau = (\pi(t - t_s)/t_p)^2 \tag{30}$$

where t_s corresponds to the peak amplitude in the time domain and t_p corresponds to the circular frequency $\omega_p = 2\pi/t_p$ which is associated with the peak amplitude in the frequency domain. Throughout the transient analysis, the response is calculated at 41 observation points equally spaced in the range of $x \in [-4, 4]$ on the surface S_F (see Figure 1). Figure 8 displays the transient surface response of the one-layer model with an irregular interface due to a vertically incident Ricker wavelet. The response can be regarded as a superposition of motion from the flat-layer model and that caused by the scattering from the layer irregularities. The scattered surface waves can be observed travelling with the shear wave velocity of the layer β_1. This is indicated by the lines ($A1 \rightarrow B1$) and ($A2 \rightarrow B2$) in Figure 8. The delay in the peaks of the transient response for sites near the origin is caused by the presence of the irregularity in the layer. Namely, the time difference between two adjacent peaks along the transient response at $x = 0$ corresponds to the double time required by a vertically propagating wave to traverse the distance from the surface to the lowest position of the irregular

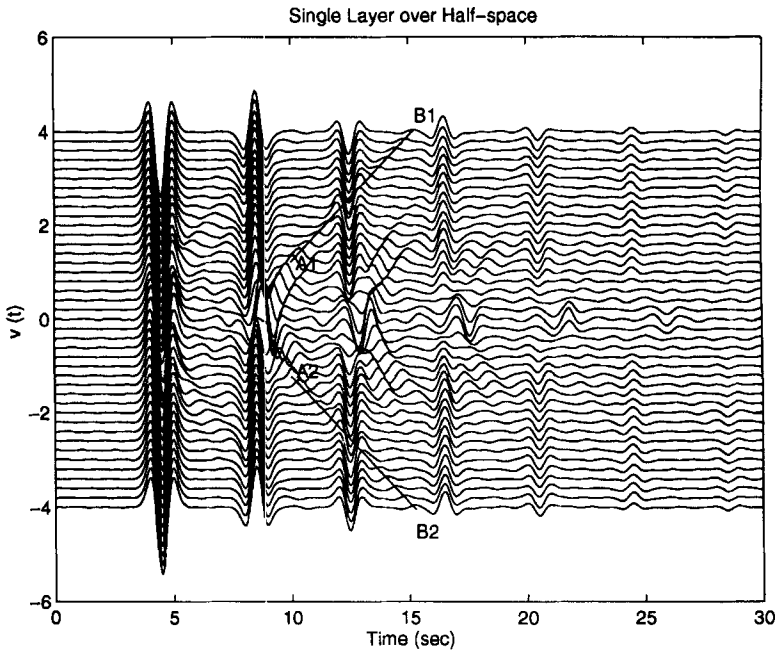

Figure 8. Transient surface response of the one-layer model due to a vertically incident Ricker wavelet. $t_p = 1{\cdot}25$ sec, $t_s = 1{\cdot}5$ sec

interface. This time is larger here than that in the flat-layer case, thus causing the gradual delay of the peaks at $x = 0$.

As expected, the peak transient surface response amplitude gradually attenuates with time due to backscattering of the waves into the half-space.

This concludes the numerical results for the one-layer model. The two-layer model is considered next.

Two-layer model

This model consists of the two cosine-shaped interfaces C_1 and C_2 defined by

$$z = \begin{cases} 0{\cdot}5 & \text{for } |x| > 0{\cdot}5 \\ 0{\cdot}5 + 0{\cdot}05(1 + \cos 2\pi x) & \text{for } |x| \leqslant 0{\cdot}5; \quad \mathbf{r} \in C_1 \end{cases} \tag{31}$$

and

$$z = \begin{cases} 1 & \text{for } |x| > 0{\cdot}5 \\ 1 + 0{\cdot}05(1 + \cos 2\pi x) & \text{for } |x| \leqslant 0{\cdot}5; \quad \mathbf{r} \in C_2 \end{cases} \tag{32}$$

The number of sources along the auxiliary surfaces $C_j^{\pm}$ are denoted by M_j and L_j, respectively. The number of collocation points along the two interfaces C_j are taken to be N_j, while the length of the interface on which the collocation points are distributed is specified by X_{n_j}. The lengths of the auxiliary surfaces C_j^- and C_j^+ over which the corresponding sources are distributed are represented by X_{m_j} and X_{l_j}, respectively, and X_{l_j} is the length of the irregular part of the interface. The maximum deviation of the irregular interface from the flat layer is denoted by d_j, and z_j is the depth of the flat-layer. The spacing between two adjacent collocation points is marked by $\mathrm{d}s_j$ and that between the auxiliary surfaces $C_j^{\pm}$ and the interface C_j by $\mathrm{d}r_j$. Here, the subscript $j = 1, 2$ corresponds to the jth interface.

Parametric error analysis. First, the transparency test for a zero-scattering condition is performed. In this test, the material properties of the two layers D_1 and D_2 are assumed to be the same as those of the half-space.

The number of the sources along the auxiliary surfaces $C_j^{\pm}$ and the collocation points along the interface C_j was adjusted until the contribution of the scattered field is found to be negligible, and the normalized surface displacement was found to be equal to one.

Based on the parametric error analysis of the one-layer model, Luco's relationship (27) and the length of interfaces $X_{n_j} \doteq 2X_{l_j}$ are assumed in this model as well. Therefore, the next test is conducted to determine the minimum number of collocation points N_1 and N_2 along the interfaces C_1 and C_2, respectively. For that purpose, four different approaches for error calculations have been designed: (i) changing first the number of collocation points N_1 and then, by repeating the error calculations for different numbers of collocation points N_2; (ii) simultaneously increasing N_1 and N_2 with $N_1 = N_2$; (iii) simultaneously increasing N_1 and N_2 with $N_1 = 2N_2$; and (iv) the error E_r is calculated with simultaneous increase of N_1 and N_2 with $N_2 = 2N_1$.

It was concluded from these tests that the surface response converges for frequencies $\Omega = 1$–4 when N_2 is between 30 and 35 while N_1 can vary from 20 to 80.

Based on the above parametric tests, the steady-state results for different frequencies and angles of incidence are presented next.

Steady-state response. For a vertical incidence the results are depicted in Figure 9. The first three frequencies at the site (0, 0) are found to be $\Omega_i = 1{\cdot}2$, 2·50 and 3·4. For corresponding flat-layer model, the resonant frequencies are $\Omega_i = 0{\cdot}88$, 2 and 3·12. The difference in the resonant frequencies between the two is attributed to the presence of the layer irregularities.

As in the one-layer case, the scattered wave field decreases in amplitude and the total wave field approaches the free-field values away from the region directly atop the layer irregularities. The surface response is found to be strongly affected by the incident wave and the site location.

This concludes the steady-state analysis of the two-layer problem. Corresponding transient results are considered next.

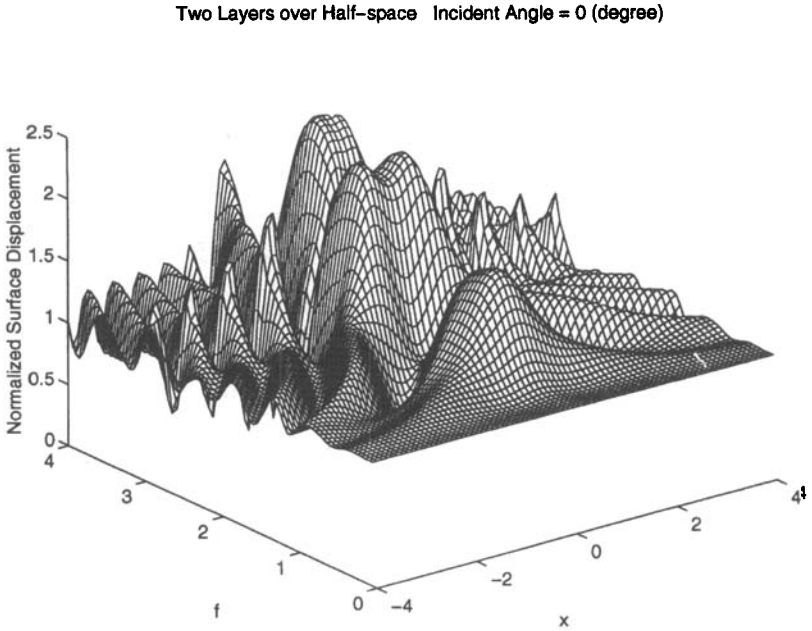

Figure 9. Normalized surface response of the two-layer model and a vertically incident harmonic wave as a function of dimensionless frequency $f(=\Omega)$ and spatial variable x. Unless stated differently, the geometry and the material properties are assumed to be $z_1 = 0{\cdot}5$, $z_2 = 1$, $X_{l_1} = X_{l_2} = 1$, $d_1 = d_2 = 0{\cdot}1$, $\beta_3 = \rho_3 = 1$, $\beta_2 = \rho_2 = 0{\cdot}5$, $\beta_1 = \rho_1 = 0{\cdot}25$. $\theta_0 = 0°$; $\Omega = 0$–4; $N_2 = 60$, $M_2 = L_2 = 24$; $N_1 = 30$, $M_1 = L_1 = 12$. Throughout the parametric error analysis of the two-layer model, $X_{n_1} = X_{n_2} = 2$, $X_{m_1} = X_{l_1} = X_{m_2} = X_{l_2} = 2{\cdot}1$; $dr_1 = 3ds_1$, $dr_2 = 3ds_2$

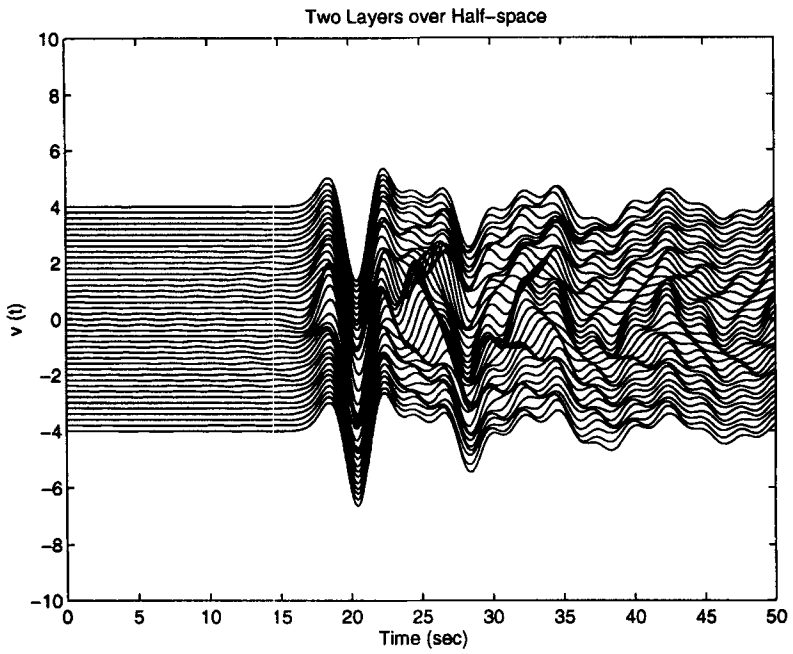

Figure 10. Transient surface response of the two-layer model due to a vertically incident Ricker wavelet. $t_p = 5$ sec, $t_s = 15$ sec

Transient response. The transient results are obtained from the steady-state response through Fourier synthesis. As before, the response is evaluated for an incident SH Ricker wavelet at 41 observation points equally spaced in the range $x \in [-4, 4]$.

Figure 10 displays the transient surface responses of a two-layer model with irregular interfaces for a vertical Ricker wavelet incidence. The oblique incidence results are omitted for the sake of briefness. Comparison with the transient response of the one-layer model leads to the following conclusions:

(i) The peak amplitude decreases with time and angle of incidence for both models while the motion amplitude of the two-layer model appears larger than that of the one-layer case.
(ii) The response patterns of the two-layer model are much more complex than those of the one-layer model.

Therefore, it appears that the presence of additional layers may change significantly the surface response when compared to a single layer model.

CONCLUSIONS

An indirect boundary integral equation approach is used to evaluate the surface response of a multilayered half-space with irregular layers to an incident SH wave. The convergence of the method is determined based on a parametric error analysis of the problem and through comparison with the results obtained by Aki and Larner.[8] Subsequently, both steady-state and transient surface response were determined for one- and two-layer models. The presented results show that the presence of layer irregularities may cause significant change in the surface response when compared with the corresponding flat-layer model response. The scattered waves affect the surface ground motion most significantly for the sites directly atop the irregularities. Away from the irregularities, the amplitude of the scattered waves decreases and the response approaches the free-field one. The surface motion was found to be very sensitive upon the nature of the incident

wave (angle of incidence and frequency), location of the observation site, and geometry and material properties of the layered medium.

ACKNOWLEDGEMENTS

This research was completed through the support from an NSF grant CMS-9412759. Special thanks are due to F. J. Sánchez-Sesma and an anonymous reviewer for their detailed and constructive comments.

REFERENCES

1. W. T. Thomson, 'Transmission of elastic waves through a stratified solid medium', *J. appl. phys.* **21**, 89–93 (1950).
2. N. A. Haskell, 'The dispersion of surface waves in multilayered media', *Bull. seismol. soc. Am.* **43**, 17–34 (1953).
3. W. M. Ewing, W. S. Jerdetzky and F. Press, *Elastic Waves in Layered Media*, McGraw-Hill, New York, 1957.
4. J. W. Dunkin, 'Computation of modal solutions in layered, elastic media at high frequencies', *Bull. seismol. soc. Am.* **55**, 335–358 (1965).
5. B. L. N. Kennett and N. J. Kerry, 'Seismic waves in a stratified half-space', *Geophys. j. roy astron. soc.* **57**, 557–583 (1979).
6. J. E. Luco and R. J. Apsel, 'On the Green's functions for a layered half-space', *Bull. seismol. soc. Am.* **73**, 909–929 (1983).
7. B. L. N. Kennett, *Seismic Wave Propagation in Stratified Media*, Cambridge University Press, New York, 1983.
8. K. Aki and K. L. Larner, 'Surface motion of a layered medium having an irregular interface due to incident plane SH waves', *J. geophys. res.* **75**, 933–954 (1970).
9. L. A. Drake, 'Love and Rayleigh waves in horizontally layered media', *Bull. seismol. soc. Am.* **62**, 1241–1258 (1972).
10. M. Bouchon, M. Campillo and S. Gaffet, 'A boundary integral equation discrete wavenumber representation method to study wave propagation in multilayered media having irregular interfaces', *Geophysics* **54**, 1134–1140 (1989).
11. X. F.Chen, 'Seismogram synthesis for multilayered media with irregular interfaces by global generalized reflection/transmission matrices method', *Bull. seismol. soc. Am.* 1696–1724 (1990).
12. K. Koketsu, B. L. N. Kennett and H. Takenaka, '2-D reflectivity method and synthetic seismograms for irregularly layered structure II. Invariant embedding approach', *Geophys. j. int.* **105**, 119–130 (1991).
13. B. L. N. Kennett, 'Reflection operator methods for elastic waves I. Irregular interfaces and regions', *Wave motion* **6**, 407–418 (1984).
14. B. L. N. Kennett, 'Reflection operator methods for elastic waves II. Composite regions and source problems', *Wave motion* **6**, 419–429 (1984).
15. P. C. Waterman, 'A new formulation of acoustic scattering', *J. acoust. soc. Am.* **45**, 1417–1429 (1969).
16. M. Dravinski, 'Scattering of plane harmonic SH waves by dipping layers of arbitrary shape', *Bull. seismol. soc. Am.* **73**, 1303–1319 (1983).
17. H. Eshraghi and M. Dravinski, 'Transient scattering of elastic waves by dipping layers of arbitrary shape. Part 1. Antiplane strain model', *Earthquake eng. struct. dyn.* **18**, 397–415 (1989).
18. H. Eshraghi and M. Dravinski, 'Scattering of elastic waves by three dimensional non-axisymmetric dipping layers', *Int. j. numer. methods eng.* **31**, 1009–1026 (1991).
19. K. Aki and P. G. Richards, *Quantitative Seismology, Theory and Methods, Vol. I*, W. H. Freeman, San Fransisco, 1980.
20. V. D. Kupradze, 'Dynamical problems in elasticity', in *Progress in Solid Mechanics*, Vol. 3, North-Holland, Amsterdam, 1963.
21. F. Ursell, 'On the exterior problems of acoustics', *Proc. Cambridge Phil. Soc.* **74**, 117–125 (1973).
22. J. Miklowitz, *The Theory of Elastic Waves*, North-Holland, New York, 1978.
23. F. J. Sanchez-Sesma, J. Ramos-Martinez and M. Campillo, 'An indirect boundary element method applied to simulate the seismic response of alluvial valleys for incident P, S and Rayleigh waves', *Earthquake eng. struct dyn.* **22**, 279–295 (1993).
24. B. Noble and J. W. Daniel, *Applied Linear Algebra*, Prentice-Hall, Englewood Cliffs, NJ, 1977.
25. T. Zhou and M. Dravinski, 'Resonance of sediment filled valleys and its prediction through an eigenvalue method', *Geophys. j. int.* **117**, 749–762 (1994).
26. N. H. Ricker, *Transient Waves in Visco-Elastic Media*, Elsevier, Amsterdam, 1977.